Depth Profiling Block Copolymer Microdomains

Christopher Harrison,[†] Miri Park,[†] Paul Chaikin,[*,†] Richard A. Register,[*,‡] Douglas H. Adamson,[§] and Nan Yao[§]

Department of Physics,Department of Chemical Engineering, and Princeton Materials Institute, Princeton University, Princeton, New Jersey 08544

Received October 30, 1997; Revised Manuscript Received January 14, 1998

ABSTRACT: We have studied the microdomain pattern in a block copolymer system using a recently developed imaging technique. We observe pronounced registry of microdomains from layer to layer, the propagation and evolution of disclinations, and novel morphologies which form at the edge of an island. The imaging of the microdomains is achieved with a nonselective etching technique which smoothly etches away sufficient material to expose the underlying microdomain layer to the surface. Using a low-voltage, high-resolution scanning electron microscope, we image the microdomains of this exposed layer which have been tagged with a staining agent.

Introduction

Diblock copolymers[1] consist of two chemically dissimilar polymer chains (i.e. blocks) which are connected by a covalent bond, typically referred to as block A and block B. The two blocks possess a relative repulsive energy of $\chi k_b T$ per monomer pair, where χ is the Flory−Huggins interaction parameter and T is temperature. Diblock copolymers with sufficiently large χN, where N is the number of monomers per chain, spontaneously microphase-separate, producing microdomains rich in one block or the other. The periodicity and the size of the microdomains are controlled by synthesizing the appropriate polymer chain length. The resulting microdomain morphology is largely determined by the relative chain lengths of blocks A and B in a given block copolymer system. Commonly reported morphologies include lamellae, cylinders, and spheres as the length of block B is shortened to less than that of block A.

The morphologies of microphase separated block copolymers have been well-examined in bulk samples by a variety of techniques, but only recently have copolymers been examined in thin films on substrates, where new effects have been observed.[2] For example, there has been a recent interest in surface-induced ordering of diblock copolymer films[3] and the role of the free surface on thin film morphology.[4] In addition, a morphological dependence on the film thickness has been observed.[5,6] Thin film structures have also become increasingly useful as lithographic masks for patterning substrates at a length scale previously inaccessible by conventional techniques.[7,8] In these studies, it has been difficult to image polymer microdomains in thin films on substrates with conventional transmission electron microscopy (TEM) techniques. A scanning electron microscopy (SEM) technique that can directly obtain real space images of these polymer systems as a function of depth within the thin film (such as the one presented in this paper) would further our understanding.

The study of block copolymers has employed many techniques during the field's history, including X-ray scattering, TEM, atomic force microscopy, and neutron reflectivity.[1] SEM, a useful tool for imaging microscopic surface features, has not been as extensively used in the study of copolymer microdomains due to its lower resolution at low voltages (1−5 kV). The imaging of polymer microdomains is necessarily done at low voltage in order to minimize charging effects and to increase contrast by decreasing the sampling depth. Recent technological developments, such as the introduction of the field emission gun SEM, have overcome these difficulties such that polymer microdomains with a typical feature size of 10 nm can now be effectively imaged. The SEM offers the advantage of studying polymer films on a substrate, such as a silicon wafer, whereas conventional TEM requires that the film be removed from the substrate and limits the samples to a thickness of less than 1 μm such that high-energy electrons can pass through the sample. The enthusiasm of the polymer community concerning the use of low-voltage, high-resolution SEM is evident in the number of recent publications.[9−13]

Until recently, electron microscopy studies of polymer microdomains have been restricted to surface observations or projections, whether plan or cross-sectional. Surface images could be obtained with SEM, but these images provide limited insight into the interior structures. Thin film sections could be microtomed for SEM or TEM analysis, but the minimum thickness appears to be approximately 70 nm, several times the thickness of typical block copolymer microdomains. TEM images of polymer microdomains are projections through the section and are often difficult to interpret when the section contains multiple layers of microdomains, particularly when the morphology changes between layers. In addition, obtaining sequentially microtomed sections of a selected region for imaging and three-dimensional reconstruction is particularly difficult. Tomographic reconstruction from TEM images is possible,[14] but it is limited to thin films without substrates and currently requires intensive computation. Therefore, we were motivated to develop a new imaging technique which allows us to examine block copolymer morphologies in thin films by imaging only a single layer of microdomains.[15] This technique has a depth resolution of 10 nm, twice as fine as the typical interlayer spacing. In

* Author to whom correspondence should be addressed.
† Department of Physics.
‡ Department of Chemical Engineering.
§ Princeton Materials Institute.

S0024-9297(97)01603-3 CCC: $15.00
Published on Web 03/10/1998

this paper, we demonstrate that this technique can provide sequential layer-by-layer images of the same region of a specimen, and we use this technique to study the microdomain pattern evolution in islands of block copolymer films.

Experimental Section

A. Material. The diblock copolymer used in this study (SB 36/11) was synthesized by standard high-vacuum anionic techniques[16] with a composition of 36 000 g/mol for the polystyrene (PS) block and 11 000 g/mol for the high 1,4-polybutadiene (PB) block such that microphase separation in the bulk produces PB cylinders in a matrix of PS. The upper glass transition temperature was measured with a Perkin-Elmer differential scanning calorimeter (model DSC 7) to be 94 °C. Thin polymer films were prepared by spin coating (spin coater manufactured by Headway Research International) toluene solutions on silicon substrates and subsequently annealing at 130 °C, well above the glass transition temperature of both blocks. In addition, thin films of homopolymer poly(2-vinylpyridine) (PVP) (Polyscience, Inc., $M_w = 200\,000$) were prepared similarly using pyridine as solvent. The silicon wafers (Silicon Quest International, 0.4 mm thick) were used as purchased except for a rinse with toluene to remove airborne contaminants. The wafers were covered with a 1−2 nm thick native oxide. The polymer film thickness was controlled by varying the solution concentration and spin speed. Film thicknesses were measured by an ellipsometer (Gaertner, Inc., model no. L116C) or an interferometer (Leica, Inc., model MPV-SP). After annealing, the PB component was selectively stained for 2 h with vapors of aqueous 4% osmium tetraoxide (Polysciences, Inc.) in order to provide contrast between the domains for electron microscopy. The osmium tetraoxide selectively stains the carbon−carbon double bonds in PB domains but does not react significantly with the PS domains.

B. Polymer Etching. Polymer film etching was performed at the Cornell Nanofabrication Facility (CNF) using a reactive ion etcher (RIE) by Applied Materials, Inc. An RIE[17] combines both the physical sputtering of an ion mill and the chemically reactive nature of a plasma etcher. The parameters used in our etching process consisted of 10 cm^3 (STP)/min of CF_4, a pressure of 2 mTorr, and a power of approximately 0.08 W/cm^2. Under these conditions, the RIE etched away approximately 12 nm of PS−PB film per minute. We found that the etching rates for both stained homopolymer PB and homopolymer PS differ by less than 10%, indicating a nonselective etching process.[15] Similar results were obtained with homopolymer PS and homopolymer PVP that was stained with iodine vapors. The etch rate varied by only a few percent over the 20 cm wide RIE chamber, resulting in a neglible variation in the etch depth for our typical sample sizes of 1 cm^2.

C. Electron Microscopy. The SEM images in this paper were obtained with a Leo Gemini 982 field emission gun SEM at CNF. SEM work was performed with an incident electron beam energy of 1 keV and by collection and addition of both secondary (SE) and backscattered electrons (BSE). The SE signal appeared to have slightly higher resolution. To optimize the SEM resolution, the working distance was very small, typically 2−3 mm. As is typical for electron microscopy, the SEM electron beam caused build-up of carbon contamination, but this is quickly etched away with CF_4 RIE and is not detrimental to image quality. However, this limits the absolute determination of the etch depth to 5 nm.

Results and Discussion

Microphase separation in a block copolymer film results in a quantized film thickness which depends on the number of microdomain layers which self-assemble internally.[18] Spin coating a film thickness slightly greater than that for two cylinder layers and annealing (in conjunction with conservation of polymer mass) produced islands which consisted of three layers of cylinders (total thickness of ∼90 nm) in a film which consisted of two layers of cylinders (∼70 nm).

The free surface of PS−PB block copolymer films is composed of PB, the lower surface tension block.[15,19] To obtain high-resolution SEM images of the top layer of cylindrical microdomains, it is necessary to first etch away this wetting layer to expose the microdomains to the surface.[15] Typically, oxygen plasma etching is used for rapid etching of carbon-based polymers, but we used a CF_4-based reactive ion etcher (RIE) in order to achieve a nonselective etching process and to etch at a sufficiently slow rate to allow control of the etch depth. The etching depth can be controlled to within a few nanometers by selecting the etching duration. Remarkably, the roughness created by CF_4 RIE has a length scale of approximately 2 nm [15] and is not detrimental to obtaining high-quality SEM images.

By varying the RIE etch depth, we found that 12 nm was the optimal thickness of material to remove to expose the internal microdomains to the surface for imaging. After etching away the free surface wetting layer across the entire film, the top layer of cylinders in both the circular island (three layers thick, defined by the brighter region in the SEM image) and the thinner film region (two layers thick) surrounding the island became visible (Figure 1A). The islands typically appeared lighter than the background at this magnification. This is a charging effect, as evidenced by reversal of this contrast at lower magnifications. The stained PB cylinders have a higher electron yield than the PS matrix due to the presence of osmium so that the PB cylinders appear lighter and the PS matrix appears darker. The cylinders can be seen lying parallel to the surface, wrapping around disclinations. At the edge of the island, one sees regions of ordered dots which may correspond to spheres or cylinders oriented perpendicular to the substrate. By continuing the depth profiling, we can discriminate between these possibilities.

To image the middle layer of microdomains, the top layer of microdomains (a thickness of approximately 20 nm) was removed with CF_4 RIE to expose the middle layer for SEM imaging. Figure 1B shows both the microdomains of the middle layer on the island (two layers thick) and the bottom layer (one layer thick) off the island. By comparing the image of the top layer (Figure 1A) and the middle layer (Figure 1B), one can observe the pronounced registry of the layers. In certain regions of Figure 1A that display white dots, black dots can be observed in Figure 1B. This is more fully examined below.

Finally, by etching away another 20 nm, the bottom layer of cylindrical microdomains is exposed (Figure 1C). Cumulatively, two layers of cylinders have been etched away, leaving only the bottom layer of cylinders on-island, while the thinner region surrounding the island has almost completely been removed, resulting in little contrast off-island. As shown in Figures 1A−C and drawn in 1D, the cylinders lie in registry from layer to layer and can adopt various orientations with respect to the edge of the island.

Despite etching away approximately 55 nm of the polymer film, there is no loss in resolution in depth profiling these microdomains, as evidenced by the same level of resolution in Figures 1A−C. The roughness introduced by etching appears to be self-healing; we have successfully etched through 240 nm thick films

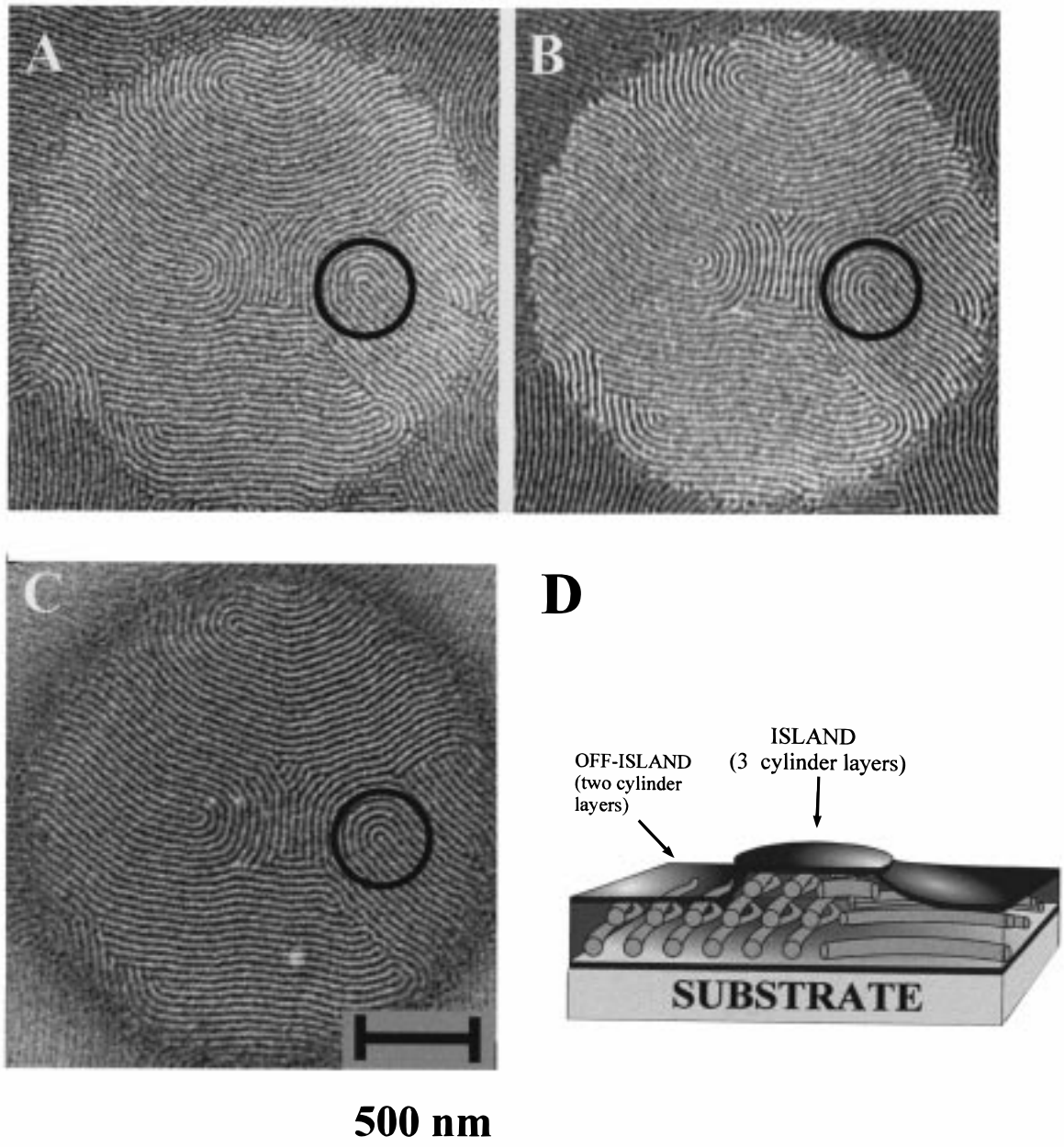

Figure 1. Depth-profiled island. Three SEM images obtained by depth profiling a circular island (center of images) containing three layers of cylinders. The island is surrounded by a region containing two cylinder layers. In images A−C, an $s = {}^1/_2$ disclination is circled which serves as a natural landmark to illustrate the packing of cylinders. (A) Top layer of cylinders is exposed for imaging after etching away PB wetting layer. Due to the OsO_4 staining, the PB cylinders are light and the PS matrix is dark. The center of the circled disclination consists of a PB cylinder. (B) Middle layer of cylinders on-island after etching away one layer of cylinders uniformly throughout the image. The center of the circled disclination consists of a PB matrix, as the middle layer of cylinders is offset from the upper layer. (C) Bottom layer of cylinders on-island after etching away two layers of cylinders (cumulative thickness of 55 nm). The center of the circled disclination consists of a PB cylinder again, mimicking the upper layer. Little contrast is seen in the region off the island, for both layers have been etched away. (D) Using these images as a guide, we present a schematic which illustrates the three layers of cylinders on-island and two layers of cylinders off-island. In addition, free and confined surface layers of PB are shown.

(∼10 layers of cylinders) without a cumulative roughening of the film.[15] Therefore, this technique would be excellent for depth profiling films to study the propagation of microdomain disclinations through distances which are at least an order of magnitude greater than their periodicity.

The pronounced registry of cylinders from layer to layer can be well-observed in the sequence of images from the depth-profiled microdomains. The circled $s = {}^1/_2$ disclination in Figure 1 serves as a natural registry mark. The disclination in the top layer (Figure 1A) consists of a terminated PB cylinder (light line) in the center around which PB cylinders progress through half a rotation. PB cylinders in sequential layers will be offset by a cylinder diameter from the previous layer (seen as a hexagonal lattice in cross-sectional view) for the most efficient packing of the copolymer chains. Consequently, directly underneath a PB cylinder in the top layer we will find a PS matrix in the middle layer. This can be seen in the circled region of the SEM image of the middle layer (Figure 1B), where the PS matrix (dark region) is seen in the middle of the disclination and the PB cylinders are offset from the middle by a cylinder diameter. Directly underneath in the bottom

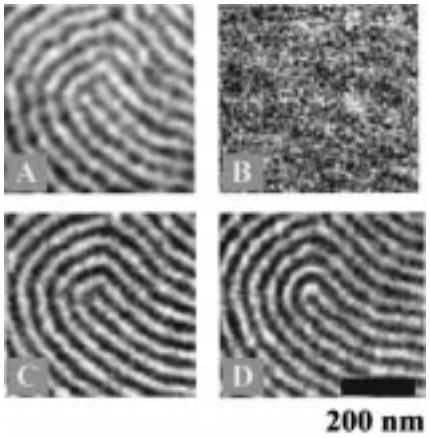

Figure 2. Transformation of a disclination revealed by depth profiling. These four SEM images obtained by depth profiling an $s = {}^1/_2$ disclination illustrate the transformation of microdomains through three layers and demonstrate the depth resolution of this technique. (A) Top layer of cylinders, showing a disclination consisting of a PS matrix in the center with two terminated PB cylinders (light lines) on either side, about which PB cylinders wind through a half-rotation. (B) Little contrast is obseved after etching to just below the top layer, for the sampling depth is too shallow to sufficiently image the middle layer which is submerged below the PS matrix. This image is used to illustrate the fineness of the depth resolution. (C) Middle layer, in which the center PB cylinder is directly underneath the center PS matrix in the top layer. (D) Bottom layer, where the PS matrix (dark region) can be seen in the middle of the disclination, about which continuous PB cylinders wind through a half-rotation. Compare to the circled disclination in Figure 1, in which the top and bottom layer mimic each other. This sequence of images suggests a mechanism by which the microdomain pattern can evolve from layer to layer.

layer (Figure 1C), there is again a PB cylinder in the center of the circled disclination, seen as a light line. For this disclination and for several others that we observed, alternating layers mimicked one another, as shown in Figure 1A−C.

Since small features such as the offset of one layer can be observed, we suggest that this technique will ultimately be useful in reconstructing three-dimensional maps of more complicated structures. This technique could find great usefulness in imaging microtomed sections of bicontinuous phases, whose structure is often difficult to interpret with TEM images of projections at various orientations.[20] In addition, this technique has proved useful in imaging the microdomain pattern of lamellae induced to orient perpendicular to a substrate.[21] Last, though we have not explored PS−PVP block copolymers in this study, the similar etch rates of homopolymer PS and stained PVP indicate that PS−PVP block copolymers could be effectively depth profiled with this technique.

Though the microdomain patterns in adjacent layers are typically quite similar, propagation through several layers allows for transformation of the pattern. One possible mechanism for pattern evolution is presented in Figure 2. Figure 2A shows the top layer of microdomains where an $s = {}^1/_2$ disclination can be observed with a PS matrix (darker) in the center. Offset from the center, two PB cylinders (lighter) terminate on either side of the PS matrix. After etching to just beneath the top layer of cylinders (an additional 10 nm), a little cylinder pattern can be discerned (Figure 2B). We use this to illustrate the resolution of the depth profiling technique, which we estimate to be approxi-

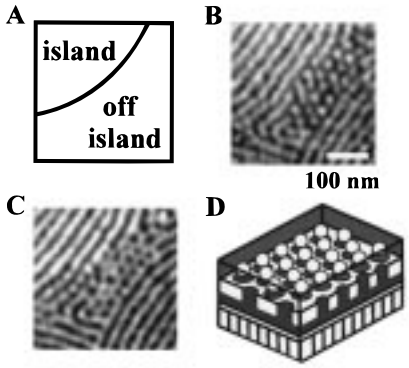

Figure 3. Novel microstructures at edge of island. These two SEM images show microstructures which typically occur at the island edge. (A) Schematic which shows the location of the island edge in the SEM images of B and C. (B) Top layer off-island, where the hexagonally packed white dots correspond to PB spheres. (C) Bottom layer off-island, in which a PB lamella can be observed to be hexagonally perforated with PS (darker). (D) A schematic drawn from B and C, in which the PB spheres lie directly above the PS perforations in the bottom PB layer. The PB is drawn light, the PS is drawn dark, and the substrate is drawn with vertical lines.

mately 10 nm when using the shallow sampling depth obtained from a 1 kV SEM beam.[15] Figure 2C shows an image of the middle layer where a terminated PB cylinder can be observed directly in the middle of the disclination. Alternating continuous PS matrix and PB cylinders can be observed to wrap around the center PB cylinder. Finally, the bottom layer (Figure 2D) shows a disclination consisting of a PS matrix in the center about which continuous PB cylinders execute a half-rotation, healing the terminated cylinders, the most energetically expensive structures, observed in the upper layer. This sequence of images suggests that patterns can evolve by transforming into topologically similar structures (both parts A and D of Figure 2 appear the same in the far field view) with different microdomain patterns as they propagate through several layers.

At the edges of the islands, we frequently observe a novel microdomain pattern which we interpret as a layer of PB spheres above a perforated PB lamella. An example of this morphology is presented in the SEM images of Figure 3, which are obtained from the edge of an island as shown in the diagram of Figure 3A. The edge of the island is located by the difference in brightness of the two regions, a differential charging effect. Several similar regions can be observed at the top and bottom edges of the island in Figure 1. After the PB wetting layer is etched away, a microdomain pattern consisting of hexagonally packed PB microdomains (white dots) can be seen at the edge of the island (center of the image of Figure 3B). After etching away another ∼20 nm of polymer film from Figure 3B to reach the next layer of cylinders, we image the middle layer on-island and the bottom layer off-island (Figure 3C). Here we see a hexagonally packed array of darker dots (PS) in a light (PB) matrix, indicating a structure resembling hexagonally perforated lamellae (HPL).[22] The PB microdomains (lighter) in the upper layer lie directly above the PS-rich regions (darker) in the lower layer, as drawn in the schematic of Figure 3D. When etched to expose the level between the upper and lower layers, similar regions produce an image without microdomain pattern contrast (not shown here). This suggests that the microdomains seen in Figure 3B are

spheres, not cylinders oriented perpendicular to the substrate, which would generate contrast regardless of the etch depth. The observed structure could not originate from a moiré-like pattern of the superposition of multiple layers because our sampling depth is approximately 10 nm, less than the diameter of the microdomains. While it is conceivable that bicontinuous cubic structures, such as the gyroid,[20] could produce similar images, our preliminary experiments indicate that block copolymers which form gyroid in bulk form lamellae when spun-coat into thin films on substrates.

We suggest that the structures presented in Figure 3 arise from the local tilting of the surface layer with respect to the substrate which necessarily occurs at the edge of the island. Assuming that the PB surface layer retains a constant thickness as it passes from the top of the island to the regions below, then this tilted surface layer at the island edge requires more PB per unit area of substrate than regions on- or off-island. Consequently, the local volume fraction of PB in the layer immediately below the surface is depleted, driving a morphological transformation from cylinders to spheres of PB. Perhaps to compensate for this local depletion, the next lower microdomain layer is transformed to a more PB-rich HPL-like structure.

We have shown that a technique which combines an RIE and a low-voltage, high-resolution SEM can be used to image each layer of microdomains independently and sequentially, allowing for true depth profiling of the morphology. We have observed a set of phenomena including the creation of an HPL-like structure at the edge of an island and the propagation and evolution of disclinations through several layers. We offer this technique as an alternative to microtoming and suggest that it will become a useful tool for researchers.

Acknowledgment. This project was greatly assisted by the instruments and the staff of the Cornell Nanofabrication Facility. This work was supported by the National Science Foundation through the Princeton Center for Complex Materials (Grant DMR-9400362). We thank Xuezhong Jiang for DSC measurements.

References and Notes

(1) Bates, F. S.; Fredrickson, G. H. *Annu. Rev. Phys. Chem.* **1990**, *41*, 525.
(2) Henkee, C. S.; Thomas, E. L.; Fetters, L. J. *J. Mater. Sci.* **1988,** *23*, 1685.
(3) Anastasiadis, S. H.; Russell, T. P.; Satija, S. K.; Majkrzak, C. F. *Phys. Rev. Lett.* **1989**, *62*, 1852.
(4) Mansky, P.; Russell, T. P. *Macromolecules* **1995,** *28*, 8092.
(5) Park, M.; Harrison, C.; Chaikin, P. M.; Register, R. A.; Adamson, D. H.; Yao, N. Volume 461: *Morphological Control in Multiphase Polymer Mixtures*, Materials Research Society, Boston, MA, Dec 2−6, 1996; Materials Research Society: Pittsburgh, PA, 1997; pp 179−184.
(6) Radzilowski, L. H.; Thomas, E. L. *J. Polym. Sci. B: Polym. Phys.* **1996,** *34*, 3081.
(7) Park, M.; Harrison, C.; Chaikin, P. M.; Register, R. A.; Adamson, D. H. *Science* **1997,** *276*, 1401.
(8) Harrison, C.; Park, M.; Chaikin, P. M.; Register, R. A.; Adamson, D. H. *J. Vac. Sci. Technol.: B*, in press.
(9) Thomas, E. L.; Vezie, D. L.; Adams, W. W. *Polymer* **1995**, *36*, 1761.
(10) Butler, J. H.; Joy, D. C.; Bradley, G. F.; Krause, S. J. *Polymer* **1995**, *36*, 1781.
(11) Joy, D. C.; Joy, C. S. *Micron* **1996**, *27*, 247.
(12) Broston, J. *Scanning* **1995,** *17*, 329.
(13) Lai, Q. J.; Simmons, S. R.; Albrecht, R. M.; Cooper, S. L. *Polym. Mater. Sci. Eng.* **1992**, *66*, 28.
(14) Spontak, R. J.; Fung, J. C.; Braunfeld, M. B.; Sedat, J. W.; Agard, D. A.; Kane, L.; Smith, S. D.; Satkowski, M. M.; Ashraf, A.; Hadjuk, D. A.; Gruner, S. M. *Macromolecules* **1996**, *29*, 4494.
(15) Harrison, C.; Park, M.; Chaikin, P. M.; Register, R. A.; Yao, N.; Adamson, D. H. *Polymer* **1998**, *39*, 2733.
(16) Morton, M.; Fetters. L. J. *Rubber Chem. Technol.* **1975**, *48*, 359.
(17) A good introduction to RIE is described by: van Roosmalen, A. J.; Baggerman, J. A. G.; Brader, S. J. H. *Dry Etching for VLSI;* Plenum Press: New York, 1991.
(18) Coulon, G.; Ausserre, D.; Russell, T. P. *J. Phys. (Paris)* **1990,** *51*, 777.
(19) Hashimoto, T.; Hasegawa, H. *Polymer* **1992,** *33*, 475.
(20) Hajduk, D. A.; Harper, P. E.; Gruner, S. M.; Honeker, C. C.; Kim, G.; Thomas, E. L.; Fetters, L. J. *Macromolecules* **1994**, *27*, 4063.
(21) Huang, E.; Mansky, P.; Russell, T. P.; Harrison, C.; Chaikin, P. M.; Register, R. A. Manuscript in preparation.
(22) Disko, M. M.; Liang, K. S.; Behal, S. K.; Roe, R. J.; Jeon, K. J. *Macromolecules* **1993**, *26*, 2983.

MA9716037